SUPPORTING MATERIAL

Locating a Lipid at the Portal to the Lipoxygenase Active Site

Betty J. Gaffney,*† Miles D. Bradshaw,† Stephen D. Frausto,† Fayi Wu,†‡ Jack H. Freed,*§ and Peter Borbat*§

†Department of Biological Science Department, Florida State University, Tallahassee, Florida 32306-4370

‡ Present address: Department of Molecular and Cellular Pharmacology, University of Miami Miller School of Medicine, 1600 NW 10th Ave., Miami, Florida 33136

§ACERT, Chemistry and Chemical Biology Department, 259 East Ave., Cornell University, Ithaca, New York 14853

*Correspondence: gaffney@bio.fsu.edu, ppb@ccmr.cornell.edu, jhf3@ccmr.cornell.edu

Content

S1. Biochemical characterization of mutant soybean seed lipoxygenase-1 (SBL1)

Table S1. Multisequence alignment of regions of soybean lipoxygenase isoforms. The residues changed to cysteine and then spin-labeled, to give R_1, are colored red and underlined. The program Cobalt (http://www.ncbi.nlm.nih.gov/tools/cobalt) was used for sequence alignment. The Protein Data Bank file for structures of these isoforms are SBL1 (1YGE) (1) SBL3 (1RRH) (2) VLXB (2IUJ) (3) and VLXD (2IUK) (3).

Alignment of helix 2   SBL1 aa 254–275 (270)

```
1YGE      LEIGTKSLSQIVQPAFESA-FDL
1RRH      LTYGLKSVSQNVLPLLQSA-FDL
2IUJ      LAYGIKSVAQDVLPVLTDA-FDG
2IUK      LTYGIKSLSHDVIPLFKSAIFQL
```

Alignment of helix 9   SBL1 aa 475–517 (480)

```
ESTIWLLAKAYVIVNDSCYHQLMSHWLNTHAAMEPFVIATHRHL
ESSIWLLAKAYVVVNDSCYHQLVSHWLNTHAVVEPFIIATNRHL
EAYIWLLAKAYVVVNDACYHQIISHWLNTHAVVEPFVIATNRHL
DSTIWLLAKAHVIVNDSGYHQLVSHWLNTHAVMEPFAIATNRHL
```

Alignment of helices 11–13   SBL1 aa 534–571 (569)

```
NMNINALARQSLINANGIIETTFLPSKYSVEMSSAVY
TMNINGLARLSLVNDGGVIEQTFLWGRYSVEMSAVVY
TMNINSLARKSLVNADGIIEKTFLWGRYSLEMSAVIY
TININGLARQSLINADGIIEKSFLPGKYSIEMSSSVY
```

Alignment of helix 15   aa SBL1 609–631 (619)

```
PYAADGLEIWAAIKTWVQEYVPLY
PYTVDGLEIWDAIKTWVHEYVFLY
PYASDGLEIWDAIKSWVEEYVSFY
PYAVDGLEIWDAIKTWVHEYVSLY
```

Alignment of helix 23   SBL1 aa 775–793 (782)

```
SKALQAFQKFGNKLKEIEE
TRALEAFKRFGNKLAQIEN
AGPLEAFKRFGKNLEEIEK
KKALEAFKRFGSKLTGIEG
```

Table S2. Enzymatic properties and iron incorporation for SBL1 and mutants

LOX-1 (# meas.)	Fe/protein (%)	K_m (mM)	k_{cat} (s^{-1})
NoCys (3)	87 ± 6	20 ± 3	215 ± 22
WT[a] (2)	85 ± 7	16 ± 2	234 ± 4
F270R$_1$ (2)	78 ± 20	13 ± 3	96 ± 29
L480R$_1$ (2)	80 ± 25	26 ± 3	245 ± 45
A569R$_1$ (4)	78 ± 4	13 ± 1	168 ± 24
A619R$_1$ (2)	84 ± 23	18 ± 5	122 ± 9
F782R$_1$ (2)	85[a]	13 ± 3	180 ± 28[a]

[a]WT is SBL1 isolated from soybeans. The F782R$_1$ sample data are for one protein sample (one iron determination) subjected to kinetic measurements twice, whereas all other data were obtained with different protein preparations measured at different times. Protein concentration was determined by absorbance at 280 nm (1 mg/ml of WT absorbance is 1.35, and of the His-tagged proteins, it is 1.28 (uncorrected for spin labeling).) A Ferene S assay was used to determine iron content (4). Values of k_{cat} were obtained from fits to data obtained with two or more separate sample preparations (see Fig. S1). One iron determination was made on each sample.

Kinetics: Enzyme kinetics data were obtained with a Cary 50 UV-Vis spectrophotometer with an Applied Photophysics RX 2000 stopped-flow rapid mixing accessory. Product formation was determined from 234-nm absorbance and ε 23,000 M^{-1}cm^{-1}. The substrates for kinetic comparison of spin labeled mutants were dilutions (3–31 μM) of ~76 μM linoleic acid with 0.003% (w/v) Tween-20 in 0.2 M sodium borate buffer, pH 9.0. Determination of inhibition by lysooleoylphosphatidylTEMPOcholine (LOPTC) used a substrate without Tween: dilutions of ~76 μM linoleic acid with 1% methanol in borate, pH 9.0. Exact substrate concentrations were determined by complete oxidation of substrate solutions. Enzyme concentration was 30 nM, and initial rates were recorded. Kinetic data, reported in Table S2 and Fig. S1, were analyzed with Visual Enzymics 2005 (http://www.softzymics.com).
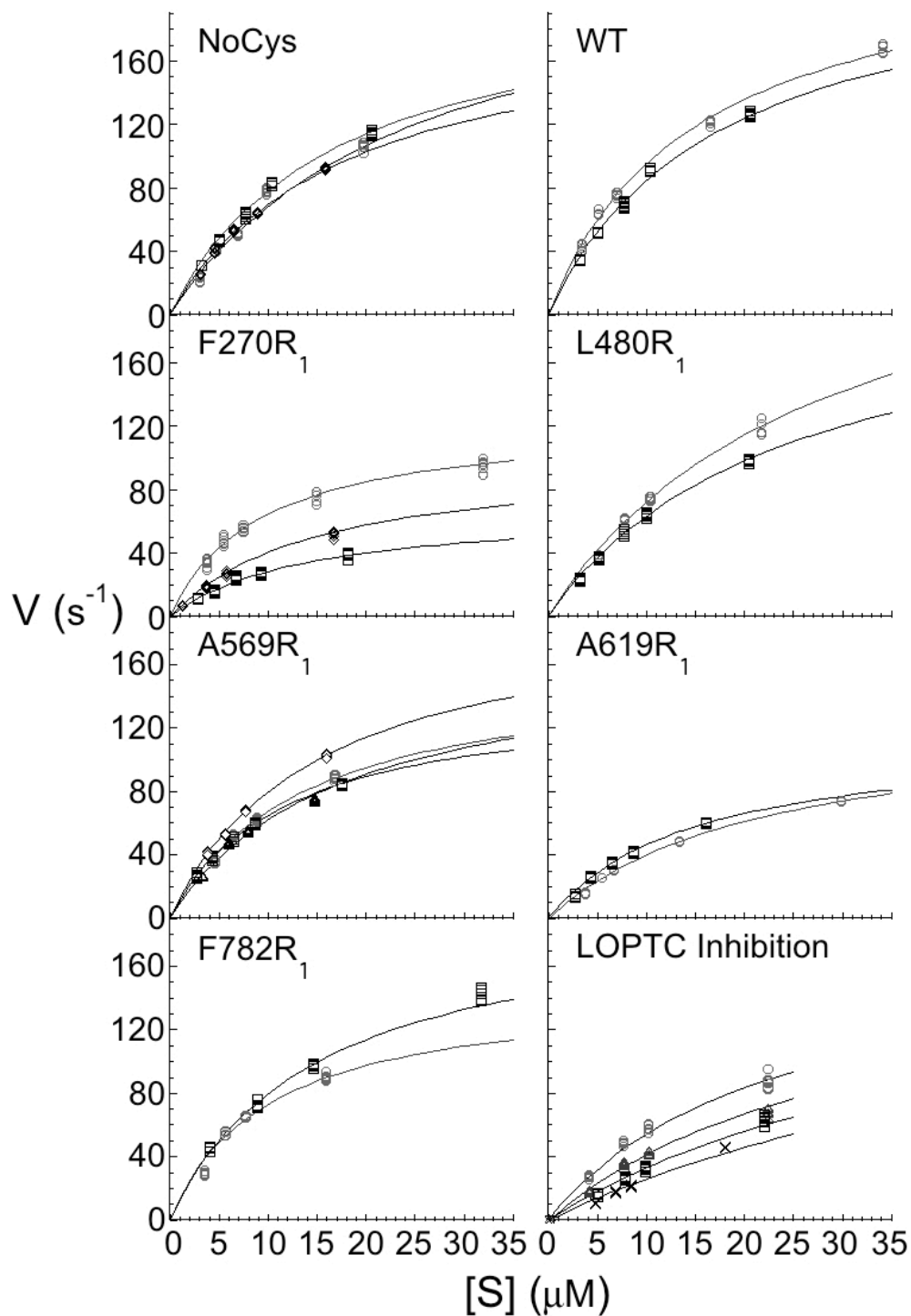
Fig. S1. Enzyme kinetics of spin labeled SBL1. Experimental details of enzyme kinetics are given in the paragraph above. For inhibition (last panel), the concentrations of LOPTC were 0, 10, 20 and 40 μM. In the inhibition experiments, the NoCys sample used was not corrected for % iron occupancy, but a single NoCys sample was used to obtain the data shown.

S2. Pulse EPR equipment and methods

Two pulse EPR sequences that work best for distance measurements were used, namely, the four-pulse double electron electron resonance (DEER) sequence, well described in the literature (5) and not detailed here, and the six-pulse double-quantum coherence (DQC), which is more sensitive, but not as well known, because the intense pulses that it requires are currently available only in very few home-built spectrometers, including the one at Cornell used in this work.
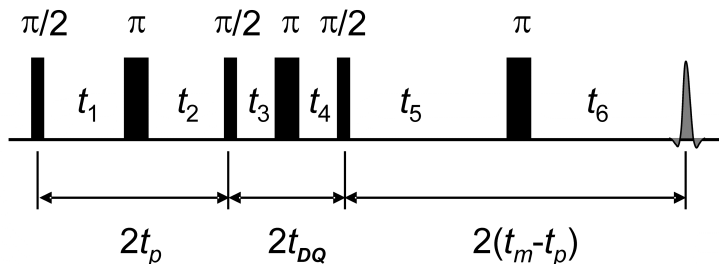

Figure S2. DQC 6-pulse sequence uses three $\pi/2$ and three π pulses separated by $t_1 = t_2 = t_p$; $t_3 = t_4 = t_{DQ}$; and $t_5 = t_m - t_p$. The 6-pulse echo is formed at time t_6 ($= t_5$) after the last pulse. The echo is recorded as a function of $t_\xi \equiv t_m - 2t_p$ by varying of t_p and t_5 in steps of Δt, such that the sum $t_p + t_5 = t_m$ is constant, as is t_{DQ}. Varying intervals in this manner does not change the position of the 6-pulse echo at $2(t_m + t_{DQ})$ after the first pulse, but t_ξ ranges from $-t_m$ to $+t_m$. The DQC modulation of the echo amplitude is isolated from the basic echo signal by application of phase cycling. The resulting signal is symmetric with respect to $t_\xi = 0$; therefore t_ξ is usually varied in the range $(0, t_m)$ or $(-\tau, t_m)$, with $\tau \ll t_m$ but sufficient to develop the maximum. (Figure from reference 7.)

The pulse EPR spectrometer used for DQC and DEER measurements is a modified version of the X/Ku band spectrometer (6). It has a quadrature mw pulse-forming channel and an additional pulse-forming channel for DEER. It is outfitted with a 4-kW Ku band TWTA (176Ku, Applied Systems Engineering) and is capable of producing intense mw pulses as short as 1 ns. The quadrature output of the receiver is recorded by a 1-Gsps dual-channel signal averager, AP240 (Agilent Technologies). Sample temperature from 4 to 300 K is provided by a CF935 liquid-helium flow cryostat (Oxford Instrument) housing a dielectric resonator. The spectrometer is capable of recording DEER and DQC signals in low-concentration samples (7)

The 6-pulse DQC sequence used in higher-resolution measurements is explained in Fig. S2 and the performance is compared to DEER in Fig. S3. The pulse lengths used were 2 and 4 ns, for $\pi/2$ and π pulses, respectively. A 64-step phase cycle (8), which is a subset of the full 256-step phase cycle, was used for DQ filtering. The phase cycle was different from that shown in the basic 64-line table on pp. 454–455 of reference (8). It is constructed as follows: the first 32 lines of the phase cycle are left as is, and then these lines are copied to make lines 33–64, but the phase of the 6th pulse is changed to *y,* and the receiver phase is inverted in this second half. No CYCLOPS steps, needed for constructing 128- and 256-step phase tables, were used.

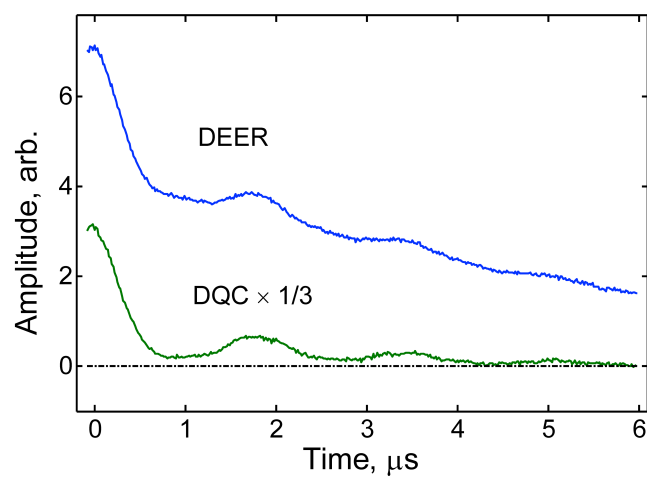An example of raw DEER and DQC data for an SBL1 double mutant.

Figure S3. Raw DQC and DEER signals from A569R$_1$/A619R$_1$ double mutant in 30% w/v glucose-d6/D$_2$O, 0.1 M Tricine buffer, pD 8.4. Protein concentrations were 4.5 mg/ml and 15.5 mg/ml, respectively. Data averaging time was 5.5 h and 13.5 h, respectively.

S3. Notes on distance distribution reconstruction for DEER and DQC

For long distances, the signal in DQC is given by

$$V(t_\xi)/V(0) \cong \int_{r_{min}}^{r_{max}} P(r)K(r,t_\xi)dr, \tag{S1}$$

and the DEER signal is

$$V(t)/V(0) = (1-p) + p\int_{r_{min}}^{r_{max}} P(r)K(r,t)dr, \tag{S2}$$

where p, determined by the pump pulse, is the "modulation depth" and the kernel K is given by

$$K(r,t) \cong \int_0^1 \cos[\gamma_e^2 \hbar t(1-3u^2)/r^3]du. \tag{S3}$$

Here, γ_e is the gyromagnetic ratio for an electron, and $\hbar$ is Plank's constant divided by 2π. In both cases, we reconstructed the distance distribution by solving Eqns. S1 and S2 using L-curve Tikhonov regularization and MEM refinement (9, 10). The latter can also fit the residual background after the decaying background is subtracted.

For an isolated spin-pair, DQC produces pure dipolar oscillations; consequently, incomplete spin labeling does not produce a background, because of the double-quantum filter. The constant background is therefore very small in DQC at low concentrations, but intermolecular couplings do contribute to the background in DQC (as in DEER), and they appear as a linear term (zero at $|t_\xi| = t_m$), which can be modified by instantaneous diffusion and nuclear spin diffusion. This background can become significant at high concentrations. It is removed as described in the literature (9, 11), but the amounts and the natures of the backgrounds in DEER and DQC differ in key ways. In DEER the background dominates the signal, and its slope (because of intermolecular contributions) can be used to estimate concentrations. The amplitude of dipolar oscillations referred to as "modulation depth" can be referenced with the amplitude at zero time and be used to estimate labeling or binding efficiency. In DQC, because of its double-quantum filter, the background at lower concentrations and evolution times is only a fraction of the dipolar signal (and of more complex origin). Such a parameter as "modulation depth" therefore cannot be defined in the same manner (or at all); hence the y-scale in DQC is in general arbitrary.

S4. Details of aligning the experimental and modeled grids by distance geometry

   Solving molecular structures on the basis of experimental (sparse) distance constraints was developed as a major tool for protein structure determination in NMR (12, 13), and it relies on distance geometry (DG) (14, 15). In the form of classical multidimensional scaling based on metric matrix, DG was applied to a small, pulsed (electron) dipolar spectroscopy (PDS) docking problem (16, 17), to determine the mode of binding of two proteins. In the present work, also carried out with PDS, accurate determination of the location of the substrate-binding site required a more elaborate effort, which involved multidimensional scaling and Procrustes analysis (PA). Using DG for a small number of points may appear an unnecessary complication, but the method is well developed, and applying it is rather straightforward. Because, with the addition of more sites, the number of possible distances rapidly increases as $N(N\text{-}1)/2$ with the number of sites, N, the methods used here become necessary. Suitable tools (*cmdscale*, *mdscale*, *procrustes*) are included in the MATLAB$^{®}$ statistical toolbox, and they were used in this work. Below, a step-by-step illustration of how this analysis was conducted is shown.

S4.1. We obtained the following set of R_1 spin-label coordinates (in Å), taken as middle points between N and O of the R_1's NO group, by averaging the rotamers from PRONOX modeling, and then used it as a reference grid in the SBL1 crystal structure (1YGE):

$$\mathbf{r}_1 = (16.26,\ 62.24,\ -0.63);\ (F270R_1)$$
$$\mathbf{r}_2 = (-8.09,\ 44.49,\ -0.48);\ (L480R_1)$$
$$\mathbf{r}_3 = (10.63,\ 42.72,\ 34.13);\ (A569R_1)$$
$$\mathbf{r}_4 = (26.66,\ 15.88,\ \ 8.96);\ (A619R_1)$$
$$\mathbf{r}_5 = (41.56,\ 28.93,\ -0.30);\ (F782R_1). \hspace{3cm} \text{(S4)}$$

S4.2 Distance matrix D_{ij} was constructed on the basis of 15 experimental distances (in Å) organized in rows/columns in the following order: $F270R_1$, $L480R_1$, $A569R_1$, $A619R_1$, $F782R_1$, LOPTC.

$$\mathbf{D}_{ij} = \begin{Vmatrix} 0 & 32.5 & 37.0 & 47.0 & 38.0 & 23.0 \\ 32.5 & 0 & 37.5 & 46.5 & 52.5 & 43.0 \\ 37.0 & 37.5 & 0 & 44.0 & 52.0 & 38.0 \\ 47.0 & 46.5 & 44.0 & 0 & 22.0 & 47.0 \\ 38.0 & 52.5 & 52.0 & 22.0 & 0 & 37.5 \\ 23.0 & 43.0 & 38.0 & 47.0 & 37.5 & 0 \end{Vmatrix}. \hspace{1.5cm} \text{(S5)}$$

S4.3 The R_1/LOPTC coordinates, $\mathbf{q}$ (in Å), from classical metric matrix DG implemented in *cmdscale.m* are

$$\mathbf{q}_1 = (-13.31\ \ 11.45\ \ -9.66);\ (F270R_1)$$
$$\mathbf{q}_2 = (-18.36\ -16.81\ -15.64);\ (L480R_1)$$
$$\mathbf{q}_3 = (-15.84\ \ -9.98\ \ 21.81);\ (A569R_1)$$
$$\mathbf{q}_4 = (\ 25.90\ -13.24\ \ \ 2.01);\ (A619R_1)$$
$$\mathbf{q}_5 = (\ 27.39\ \ \ 5.85\ \ -3.43);\ (F782R_1)$$
$$\mathbf{q}_6 = (\ -5.79\ \ 22.73\ \ \ 4.92);\ (LOPTC). \hspace{2.5cm} \text{(S6)}$$

The eigenvalues (2072, 1169, 787, 142.5, 0.0, –2.4) are dominated by the largest three, all positive, indicating that experimental errors and distance-reconstruction uncertainties do not result in distances that are far from representing points in $\mathbb{R}^3$. The resulting shape, however, is yet to be aligned with the reference grid.

S4.4. The error matrix, the difference (in Å) between the experimental distance matrix D_{ij} and the distances (disparity matrix) Δ_{ij}, calculated by embedding of D_{ij} into $\mathbb{R}^3$ by multidimensional scaling based on *mdscale.m*:

$$\mathbf{D} - \mathbf{\Delta} = \begin{Vmatrix} 0 & 3.17 & -1.15 & -0.79 & -3.56 & 3.10 \\ 3.17 & 0 & -0.65 & -1.29 & 0.00 & -3.31 \\ 1.15 & -0.65 & 0 & -2.31 & -0.50 & -0.15 \\ -0.79 & -1.29 & -2.31 & 0 & 2.10 & -1.02 \\ -3.56 & 0.00 & -0.50 & 2.10 & 0 & -0.65 \\ 3.10 & -3.31 & -0.15 & -1.02 & -0.65 & 0 \end{Vmatrix}. \qquad \text{(S7)}$$

This matrix may indicate that a small SBL1 restructuring could occur upon LOPTC binding, or as a consequence of the pH difference between that of the PDS samples and of the crystallographic pH, but characterizing it in detail would require further, more extensive study. (Note that the solution stress is small, $8.5 \cdot 10^{-7}$, and the stress for distances not including those to LOPTC is just $1.3 \ 10^{-16}$, with the maximum error of 0.52 Å.) Eigenvalues determined by *cmdscale* are 1894, 775, 692, 18, 0).

S4.5. The R_1 coordinates, $\mathbf{q}$, were transformed onto the PRONOX reference grid by *procrustes* $\rho_k = \mathbf{R}\mathbf{q}_k + \mathbf{t}$. $\mathbf{R}$ is an orthogonal matrix (rotations and reflections), and $\mathbf{t}$ is a translation vector.

$$
\begin{aligned}
\rho_1 &= (16.46, \ 60.84, \ 0.85); \ (F270R_1) \\
\rho_2 &= (-8.03, \ 44.71, \ 0.27); \ (L480R_1) \\
\rho_3 &= (\ 8.06, \ 45.71, \ 34.85); \ (A569R_1) \\
\rho_4 &= (28.87, \ 15.11, \ 7.02); \ (A619R_1) \\
\rho_5 &= (41.67, \ 27.88, \ -1.32); \ (F782R_1).
\end{aligned}
\qquad \text{(S8)}
$$

The error vectors $\delta\mathbf{r}_k = \rho_k - \mathbf{r}_k$ between the vertices of the reference and the experimental grids are

$$
\begin{aligned}
\delta\mathbf{r}_1 &= (\ 0.20, \ -1.40, \ 1.48); \ (F270R_1) \\
\delta\mathbf{r}_2 &= (\ 0.06, \ 0.22, \ 0.75); \ (L480R_1) \\
\delta\mathbf{r}_3 &= (-2.58, \ 2.99, \ 0.72); \ (A569R_1) \\
\delta\mathbf{r}_4 &= (\ 2.21, \ -0.77, \ -1.94); \ (A619R_1) \\
\delta\mathbf{r}_5 &= (\ 0.11, \ -1.05, \ -1.02); \ (F782R_1).
\end{aligned}
\qquad \text{(S9)}
$$

The dissimilarity of the two grids after alignment, $d = 0.0093$, was calculated by *procrustes* as

$$d = \sum_{ki} \delta r_{ki}^2 \Big/ \sum_{k,i} \overline{q}_{ki}^2 , \qquad\qquad (S10)$$

where i = 1,…3 and $\overline{q}_{ki}$ are the centered $\mathbf{q}_k$. The dissimilarity is small, indicating good, although not ideal, alignment. The largest difference $\boldsymbol{\delta r}_k$ is observed for the rotamer-rich site A569R$_1$, where χ_2 is less certain than for other sites, but it has a small effect on the outcome.

S4.6. LOPTC spin location after application of the rotation, **R,** and translation, **t,** to $\mathbf{q}_6$ (LOPTC) is

$$\boldsymbol{\rho}_6 \text{(LOPTC)} = (\mathbf{\textit{30.4, 62.18, 12.2}}), \text{ Å.} \qquad\qquad (S11)$$

S4.7. This result (Eqn S11) is taken as the location of the LOPTC spin in SBL1, but it does not indicate the accuracy of the solution or whether this location is indeed the most probable one or is just close to it. The result depends on finding an accurate set of reference points, as well as on the experimental distances that are distributed. Because varying experimental distances yield different $\boldsymbol{\rho}_6$, giving a 1σ range of solutions requires determining the probability that LOPTC is found at any given point by varying experimental distances within their ranges. Changing the position of one of the R$_1$ side-chains affects its distances from the rest; i.e., the distances are correlated in some way. This relationship is complex and unknown from the experiment, where distance distributions do not reveal such dependencies, but real configurations do represent polyhedrons, and consequently a set of distances, which should be embeddable in the 3D space with minimal stress. The stress can be upper-bounded, permitting the sets that do not correspond to points in the 3D space to be ignored. In addition, the alignment of a solution with the reference grid should be reasonably tight. Therefore, the dissimilarity of two grids should also be assigned an upper bound. We used a standard Kruskal's stress criterion,

$$stress(\mathbf{X}, \mathbf{D}) = \sqrt{\sum_{i>j} (x_{ij} - d_{ij})^2 \Big/ \sum_{i>j} d_{ij}^2} , \qquad\qquad (S12)$$

in which **D** are experimental dissimilarities, and **X** are the dissimilarities of the embedding result. Because the experimental distance is given by a distance distribution, $P(r)$, the Monte Carlo method using random sets of distances was applied. The probability p of a particular configuration was taken as a product of Gaussian functions, normalized to unity amplitude, with means and RMSD estimated from $P(r)$'s. Only configurations with $p > 10^{-3}$ were considered. Because varying the experimental distances yields different $\boldsymbol{\rho}_6$, the experimental distances were allowed to vary in the 2RMSD range, and Monte Carlo trials were made on a large (100 Å)^3 grid with 0.5-Å grid spacing, giving a probability to each voxel after normalization with the sum over the grid. Only about 5–10% of trials were accepted because of stress and dissimilarity constraints. The 3D plotting of isosurfaces at the 2σ level (in one dimension) revealed a nearly ellipsoid shape, with radii $(a, b, c) = (2.2, 4.7, 6)$ Å.

S5. Test for LOPTC occupying the cavity in opposite orientation

Even though we found only one solution by DG, we must still determine whether a small fraction of LOPTC resides in the cavity in the opposite orientation, i.e. "head first." In this case we expect a relatively short distance to $L480R_1$ compared to ~43 Å in the orientation we have determined. To test this possibility, we recorded the DEER signal at a high signal-to-noise ratio using a 1.2 µs time scale.
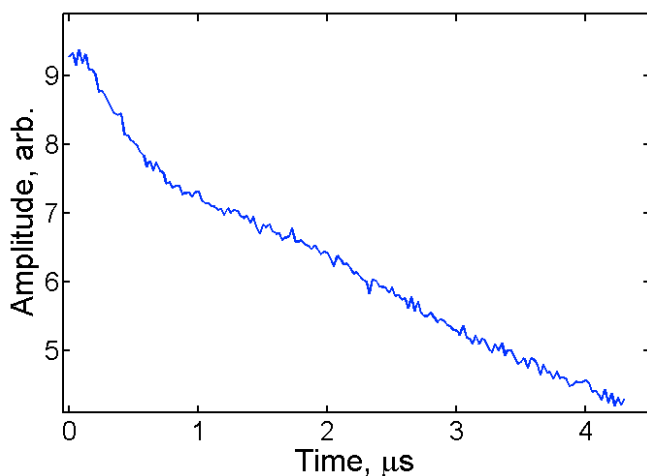

Figure S4. Raw DEER data recorded on 80 µM $L480R_1$ with bound LOPTC and 4.5 µs evolution time data. The time-domain signal corresponds to a single distance distributed around ~43 Å. Data-averaging time was 3 h; temperature was 60 K. The presence of a smaller distance was tested as shown in the Fig. S4.
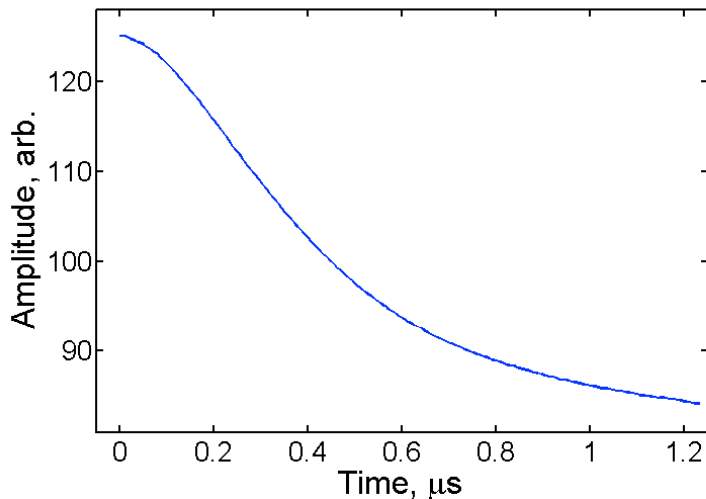

Figure S5. High-signal-to-noise-ratio DEER data for 80 µM $L480R_1$ with LOPTC bound. The time domain signal did not indicate the presence of the short-distance component (≤25 Å) expected for the "head first" orientation of LOPTC. Approximation of data by a low-order polynomial leaves the residual corresponding to no more than 0.5% of bound LOPTC at a small distance from $L480R_1$.

Supporting References

1. Minor, W., J. Steczko, B. Stec, Z. Otwinowski, J. T. Bolin, R. Walter, and B. Axelrod. 1996. Crystal structure of soybean lipoxygenase L-1 at 1.4 Å resolution. *Biochemistry* 35:10687–10701.
2. Skrzypczak-Jankun, E., R. A. Bross, R. T. Carroll, W. R. Dunham, and M. O. Funk. 2001. Three-dimensional structure of a purple lipoxygenase. *J. Am. Chem. Soc.* 123:10814–10820.
3. Youn, B., G. E. Sellhorn, R. J. Mirchel, B. J. Gaffney, H. D. Grimes, and C. Kang. 2006. Crystal structures of vegetative soybean lipoxygenase VLX-B and VLX-D, and comparisons with seed isoforms LOX-1 and LOX-3. *Proteins* 65:1008–1020.
4. Zabinski, R., J. M. Wood, P. M. Champion, and E. Munck. 1972. Kinetic and Mossbauer studies on mechanism of protocatechuic acid 4,5-oxygenase. *Biochemistry* 11:3212–3219.
5. Jeschke, G., and Y. Polyhach. 2007. Distance measurements on spin-labelled biomacromolecules by pulsed electron paramagnetic resonance. *Phys. Chem. Chem. Phys.* 9:1895–1910.
6. Borbat, P. P., R. H. Crepeau, and J. H. Freed. 1997. Multifrequency two-dimensional Fourier transform ESR: an X/Ku-band spectrometer. *J. Magn. Reson.* 127:155–167.
7. Borbat, P. P., and J. H. Freed. 2012. Pulse dipolar ESR: distance measurements. *In* Structural Information from Spin-Labels and Intrinsic Paramagnetic Centres in the Biosciences. Structure and Bonding. J. Harmer and C. Timmel, editors. Springer, Berlin, Heidelberg. In press. doi: 10.1007/430_2012_82.
8. Borbat, P. P., and J. H. Freed. 2000. Double-quantum ESR and distance measurements. *In* Biological Magnetic Resonance, Vol. 19. L. J. Berliner, G. R. Eaton, and S. S. Eaton, editors. Kluwer Academics/Plenum Publishers, New York. 383–459.
9. Chiang, Y. W., P. P. Borbat, and J. H. Freed. 2005. The determination of pair distance distributions by pulsed ESR using Tikhonov regularization. *J. Magn. Reson.* 172:279–295.
10. Chiang, Y. W., P. P. Borbat, and J. H. Freed. 2005. Maximum entropy: a complement to Tikhonov regularization for determination of pair distance distributions by pulsed ESR. *J. Magn. Reson.* 177:184–196.
11. Borbat, P. P., H. S. McHaourab, and J. H. Freed. 2002. Protein structure determination using long-distance constraints from double-quantum coherence ESR: study of T4 lysozyme. *J. Am. Chem. Soc.* 124:5304–5314.
12. Havel, T., and K. Wuthrich. 1984. A distance geometry program for determining the structures of small proteins and other macromolecules from nuclear magnetic-resonance measurements of intramolecular ^{1}H-^{1}H proximities in solution. *Bull. Math. Biol.* 46:673–698.
13. Havel, T. F., and K. Wuthrich. 1985. An evaluation of the combined use of nuclear magnetic-resonance and distance geometry for the determination of protein conformations in solution. *J. Mol. Biol.* 182:281–294.
14. Havel, T. F., I. D. Kuntz, and G. M. Crippen. 1983. The theory and practice of distance geometry. *Bull. Math. Biol.* 45:665–720.
15. Najfeld, I., and T. F. Havel. 1997. Embedding with a rigid substructure. *J. Math. Chem.* 21:223–260.

16. Borbat, P. P., K. Surendhran, M. Bortolus, P. Zou, J. H. Freed, and H. S. McHaourab. 2007. Conformational motion of the ABC transporter MsbA induced by ATP hydrolysis. *PLoS Biol.* 5:2211–2219.
17. Park, S. Y., P. P. Borbat, G. Gonzalez-Bonet, J. Bhatnagar, A. M. Pollard, J. H. Freed, A. M. Bilwes, and B. R. Crane. 2006. Reconstruction of the chemotaxis receptor-kinase assembly. *Nat. Struct. Mol. Biol.* 13:400–407.